AD-A110 949 DEFENCE RESEARCH ESTABLISHMENT VALCARTIER (QUEBEC) F/G 20/5
PROPAGATION MODEL OF ADAPTIVELY CORRECTED LASER BEAMS IN TURBUL--ETC(U)
OCT 81 L R BISSONNETTE
UNCLASSIFIED DREV-4200/81 NL

1 OF 1
AD
A110949

END
DATE
FILMED
8-82
DTIC

END
DATE
FILMED
8-82
DTIC

(3)

LEVEL II

(12) 45

Centre de Recherches pour la Défense

Defence Research Establishment

Valcartier, Québec

BUREAU - RECHERCHE ET DEVELOPPEMENT
MINISTERE DE LA DEFENSE NATIONALE
CANADA

RESEARCH AND DEVELOPMENT BRANCH
DEPARTMENT OF NATIONAL DEFENCE
CANADA

404945

CRDV R-4200/81 UNCLASSIFIED DREV R-4200/81
DOSSIER: 3633B-007 FILE: 3633B-007

PROPAGATION MODEL OF ADAPTIVELY CORRECTED LASER BEAMS IN TURBULENCE

by

L.R. Bissonnette

CENTRE DE RECHERCHES POUR LA DEFENSE

DEFENCE RESEARCH ESTABLISHMENT

VALCARTIER

Tel: (418) 844-4271

Québec, Canada

October/octobre 1981

NON CLASSIFIE

RESUME

Ce rapport décrit un modèle mathématique pour la solution du problème de propagation de faisceaux laser se déplaçant dans l'atmosphère turbulente et corrigés par une optique adaptable. Celle-ci est simulée à l'aide d'une relation mathématique simple mais suffisamment générale pour représenter la plupart des systèmes existants. Le modèle tient compte également des effets de vibration du faisceau et de cohérence partielle de la source. La méthode permet de prédire les profils de l'intensité moyenne et de la variance de l'intensité pour des niveaux arbitraires de scintillation. On présente quelques solutions typiques pour des faisceaux de longueur d'onde de 3.8 et 10.6 μm. Ces résultats illustrent les performances, après propagation dans la turbulence, d'un système d'optique adaptable en fonction de la longueur d'onde, du nombre d'éléments actifs et du niveau de bruit. (NC)

ABSTRACT

This report describes a mathematical model for solving the propagation problem of laser beams traveling in atmospheric turbulence and corrected by adaptive optics. The modeling of the adaptive optics is mathematically simple but sufficiently general to encompass the majority of the existing systems. The model also includes the effects of beam jitter and partial coherence of the source. The method allows the prediction of the average irradiance and the irradiance variance beam profiles for arbitrary scintillation levels. Typical solutions are presented for 3.8-and 10.6-μm laser beams. These results illustrate the performance, after propagation in turbulence, of an adaptive system as a function of the wavelength, the number of active elements and the noise level. (U)

TABLE OF CONTENTS

1.0 INTRODUCTION

Atmospheric turbulence seriously affects the propagation of laser beams. The refractive index turbulence induces random phase and amplitude modulations which cause the beam to scintillate, to lose its spatial and temporal coherence, to wander about its axis, and to spread out. A prediction model for the average irradiance and the irradiance variance profiles of laser beams traveling in such a turbulent medium was developed at the Defence Research Establishment Valcartier (DREV) and is described in Refs. 1, 2 and 3. The principal advantages of the model are that it is applicable at arbitrary scintillation levels and that the solutions can be computed by straightforward finite-difference techniques. The results of Refs. 1 to 3 show that the numerical solutions agree very well with the experimental data and that the classical perturbation solutions are recovered in the weak scintillation limit.

In this report, we modify the DREV model to include the corrective effect of adaptive optics which has now been proven quite efficient in compensating for wave front distortions induced by turbulence. The many aspects of this new technology are well reviewed in Ref. 4. The technique will likely have an important impact on several optical and infrared applications in the atmosphere. It is therefore essential for the design and analysis of upcoming systems to be able to simulate adaptive optics. The existing numerical codes in the literature concern mainly the simulation of the optical systems; propagation is mostly reduced to computer-generated random input signals. This report addresses itself to the intrinsic propagation problem. The constitutive closure relations of Refs. 1 to 3 are rederived to model the operation of adaptive optics. The approach neglects technical particularities but this is done for the sake of generality and no

problem is foreseen for dealing with specific systems. The purpose is to demonstrate the efficiency of the DREV model to simulate the propagation of adaptively corrected laser beams in turbulence.

Section 2.0 reviews the basic features of our propagation model. Section 3.0 describes the modifications made to simulate adaptive optics, beam jitter, and partial coherence of the source. Section 4.0 proposes a finite-difference algorithm and Section 5.0 presents and compares calculation results at two wavelengths, λ = 10.6 μm and 3.8 μm.

This work was performed at DREV between October 1979 and June 1980 under PCN 33B07, Atmospheric Propagation of Laser Beams.

2.0 PROPAGATION MODEL

Our mathematical model for beam propagation in turbulence is described in Refs. 1, 2 and 3. The model is in the form of a closed set of simultaneous partial differential equations for the first- and second- order statistical moments of the complex wave amplitude. From the solution of these equations, the average irradiance and the irradiance variance beam profiles can be easily calculated.

The basic features of the model are recalled from Ref. 3. First, the instantaneous random scalar electric field E of the assumed monochromatic wave propagating in the z-direction under negligible polarization effects is written as follows:

$$E = A \exp\left[jk(z + \phi) - j\omega t\right], \qquad [1]$$

where A is a complex amplitude, $k\phi$ is a phase function, $k = n_o\omega/c$ is the optical wave number, n_o is the unperturbed index of refraction, ω is the optical angular frequency of the source, c is the speed of light in free space and $j = \sqrt{-1}$. Second, eq. 1 is substituted for E in the scalar-wave equation which, under the paraxial approximation and after separation for A and ϕ, becomes

$$\left(\frac{\partial}{\partial z} + \mathbf{V}\cdot\nabla\right)\mathbf{V} = \nabla(N - n_o)/n_o\,, \qquad [2]$$

$$\left(\frac{\partial}{\partial z} + \mathbf{V}\cdot\nabla\right)A + \frac{1}{2}A\nabla\cdot\mathbf{V} - \frac{j}{2k}\nabla^2 A = 0\,, \qquad [3]$$

where N is the instantaneous random index of refraction, $\underset{\sim}{\nabla}$ is the gradient operator in the plane normal to the o-z axis, and $\underset{\sim}{V} = \underset{\sim}{\nabla}\phi$. In obtaining eq. 2, it was assumed that $|N-n_o|/n_o \ll 1$, which is well verified in atmospheric turbulence. Third, the random functions are written as sums of an average and a fluctuating part, i.e.

$$N = \langle N \rangle + n;\ \langle n \rangle = 0, \qquad [4]$$

$$\mathbf{V} = \langle \mathbf{V} \rangle + \mathbf{v};\ \langle \mathbf{v} \rangle = 0, \qquad [5]$$

$$A = \langle A \rangle + a;\ \langle a \rangle = 0, \qquad [6]$$

where the pointed brackets denote ensemble averaging. Then, the equations for the first- and second- order statistical amplitude moments are easily derived from eqs. 2 to 6, but they contain more unknowns than there are equations. This is the classical closure problem which affects the treatment of turbulent phenomena governed by nonlinear or quasi-linear stochastic equations such as eqs. 2 and 3. For the present application, this problem was solved in Ref. 3 where the unknown moments are mathematically related to the first- and second-order amplitude moments, thus closing the set of equations. For a wave originally

focused at z = F in a transversely statistically homogeneous medium, i.e. $\underset{\sim}{\nabla} < N > = \underset{\sim}{\nabla} < \underset{\sim}{v}.\underset{\sim}{v} > = 0$, the resulting moment equations are

$$\frac{\partial < A >}{\partial z} + \frac{\mathbf{r}}{z-F} \cdot \nabla < A > + \frac{< A >}{z-F} + \frac{1}{2} K(z) < A > - \mathbf{R}(z) : \nabla\nabla < A > - \frac{j}{2k} \nabla^2 < A > = 0. \quad [7]$$

$$\frac{\partial < aa^* >}{\partial z} + \frac{\mathbf{r}}{z-F} \cdot \nabla < aa^* > + \frac{< aa^* >}{z-F} - \frac{1}{2} \mathrm{Real}\left\{\mathbf{R}(z)\right\} : \nabla\nabla < aa^* >$$

$$- \frac{\Theta^2 z}{2} \frac{F}{F-z} \nabla^2 < aa^* > = 2\,\mathrm{Real}\left\{(\mathbf{R}(z) \cdot \nabla < A >) \cdot \nabla < A >^*\right\}$$

$$+ \mathrm{Real}\left\{K(z)\right\} < A > < A >^*. \quad [8]$$

$$\frac{\partial < aa >}{\partial z} + \frac{\mathbf{r}}{z-F} \cdot \nabla < aa > + \frac{< aa >}{z-F} + j\,T(z) < aa > - \frac{1}{2} \mathbf{R}(z) : \nabla\nabla < aa >$$

$$- \frac{j}{4k} \nabla^2 < aa > = 2\,(\mathbf{R}(z) \cdot \nabla < A >) \cdot \nabla < A > + K(z) < A >^2. \quad [9]$$

where θ is the diffractional far-field half-angle beam divergence. For a Gaussian beam with an irradiance e-folding radius r_o, $\theta = 1/kr_o$. The coefficients $\underset{\approx}{R}(z)$, K(z) and T(z), which constitute the basis of the closure model, are given by

$$\mathbf{R}(z) = \frac{jk}{2\pi} \int_0^z \frac{du}{u-z} \iint_{-\infty}^{\infty} d^2\mathbf{s} < \mathbf{v}(z,\mathbf{r})\,\mathbf{v}(u,\mathbf{s}) > \exp\left[\frac{jk}{2(z-u)} \frac{F+z-2u}{F-u} \left| \frac{F-u}{F-z} \mathbf{r} - \mathbf{s} \right|^2\right]. \quad [10]$$

$$K(z) = \frac{jk}{4\pi} \int_0^z \frac{du}{u-z} \iint_{-\infty}^{\infty} d^2\mathbf{s}\, \nabla_r \nabla_s : < \mathbf{v}(z,\mathbf{r})\,\mathbf{v}(u,\mathbf{s}) > \exp\left[\frac{jk}{2(z-u)} \frac{F+z-2u}{F-u} \left| \frac{F-u}{F-z} \mathbf{r} - \mathbf{s} \right|^2\right]. \quad [11]$$

$$T(z) = \begin{cases} C \dfrac{F-z/2}{F-z} \dfrac{1}{z}\,; & z \leqslant z_A, \\[2ex] C \dfrac{F-z/2}{F-z} \dfrac{z}{z_A^2}\,; & z > z_A, \end{cases} \quad [12]$$

where $C = 0.15 - 0.01\,j$ is a numerical empirical constant and $z_A = n_o^{12/11}/C_n^{12/11} k^{7/11}$ is the propagation scale characteristic of turbulence fading. It is noted that the semi-empirical eq. 12 is not required to solve for the average irradiance but only for the irradiance variance. This empirical input could be omitted only at the expense of a much higher level of complexity, namely the solution for the amplitude covariance function which satisfies a partial differential equation of at least two more independent variables. Hence, in view of the simplicity and accuracy of eq. 12, as demonstrated by the results of Refs. 1 to 3, the need for the universal empirical constant C is considered acceptable.

The quantities of interest are the average irradiance

$$\langle I \rangle = \langle A \rangle \langle A \rangle^* + \langle aa^* \rangle, \qquad [13]$$

and the irradiance variance which, under the approximation of Gaussian statistics for the complex amplitude A (e.g. Ref. 5), is given by

$$\begin{aligned}\sigma_I^2 = {} & \langle aa^* \rangle^2 + \langle aa \rangle \langle aa \rangle^* + 2 \langle A \rangle \langle A \rangle^* \langle aa^* \rangle \\ & + \langle A \rangle \langle A \rangle \langle aa \rangle^* + \langle A \rangle^* \langle A \rangle^* \langle aa \rangle. \end{aligned} \qquad [14]$$

The coefficients $\underset{\approx}{R}(z)$ and K(z) are functions of the covariance of the random vector $\underset{\sim}{v}$. The stochastic equation for $\underset{\sim}{v}$ is easily derived from eqs. 2 to 5. For an originally spherical phase front focused at z = F, it is given by

$$\frac{\partial \mathbf{v}}{\partial z} + \frac{\mathbf{r}}{z - F} \cdot \nabla \mathbf{v} + \frac{\mathbf{v}}{z - F} + \mathbf{v} \cdot \nabla \mathbf{v} = \nabla n / n_0 \,, \qquad [15]$$

which is the paraxial form of the eikonal equation of geometrical optics. Hence $\underset{\sim}{v}(z,\underset{\sim}{r})$ is the component, in the transverse plane, of the unit vector parallel to the geometrical ray passing through the point $(z, \underset{\sim}{r})$ or, in other words, $\underset{\sim}{v}(z, \underset{\sim}{r})$ is the vector angle subtended by the geometrical ray at $(z, \underset{\sim}{r})$.

In Ref. 3, the expressions for $\underset{\approx}{R}(z)$ and $K(z)$ were derived from the solution of eq. 15, with the boundary condition $\underset{\sim}{v}(o, \underset{\sim}{r}) = 0$. In the present report, we will rederive these expressions to account for the action of an adaptive optical system that produces random fluctuations of $\underset{\sim}{v}$ at $z = 0$ in response to some corrective criterion. Therefore, our task will be, first, to determine the statistics of $\underset{\sim}{v}(o, \underset{\sim}{r})$, second, to solve eq. 15 with this new boundary condition, and finally, to derive the resulting expressions for $\underset{\approx}{R}(z)$ and $K(z)$. The solution to the propagation problem is then straightforward with eqs. 7 to 9 forming a closed set of equations easily solved by finite difference techniques.

3.0 MODELING OF $\underset{\approx}{R}(z)$ AND $K(z)$

In this section, we derive the coefficient $\underset{\approx}{R}(z)$ and $K(z)$ for an adaptively corrected beam propagating in homogeneous Kolmogorov's turbulence. Also derived are the contributions to $\underset{\approx}{R}(z)$ and $K(z)$ resulting from partial coherence of the source and residual jitter of the transmitting optics.

3.1 Adaptive Optics Model

The adaptive optical system is assumed to derive its information from the radiation returned by an unresolved glint on the target illuminated by the outgoing beam at focal distance $z = F$. The geometry

of the returned signal is therefore that of an originally spherical wave and is schematically illustrated in Fig. 1. It is evident that an auxiliary point source could also replace the reflecting glint.

The quantity of interest, or the information available to the adaptive system, is the state of distortion, at the transmitter plane, of the phase of the returned spherical wave. In the notation used here, this is measured by the random ray angle $\underset{\sim}{v}$ which satisfies eq. 15. Since $|\underset{\sim}{v}|<<1$ for atmospheric turbulence, the nonlinear term in eq. 15 can be neglected to give

$$\frac{\partial v}{\partial \xi}+\frac{r'}{\xi}\frac{\partial v}{\partial r'}+\frac{v}{\xi}=\nabla n/n_0 , \qquad [16]$$

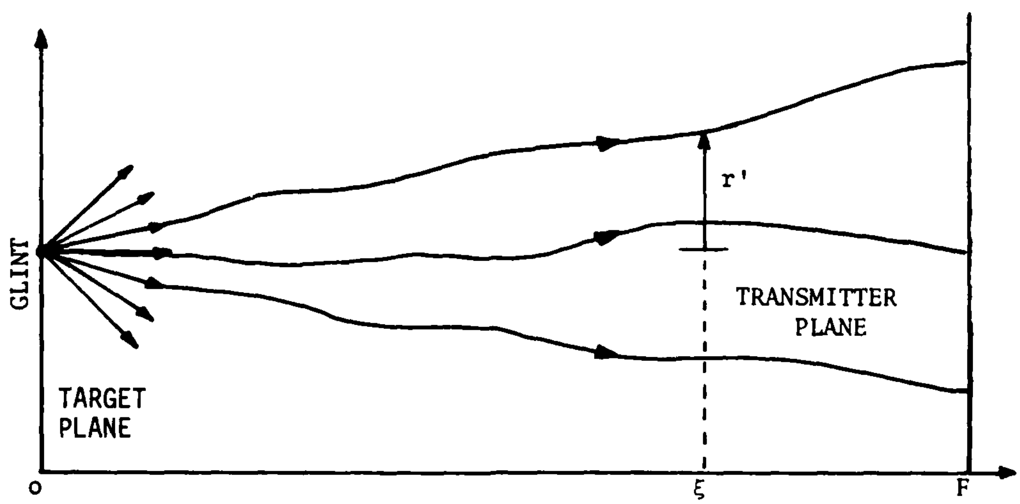

FIGURE 1 - Schematic representation of the reflected wave from a glint on the target

where the variables ξ and r' are defined in Fig. 1. Solving with the boundary condition $\underset{\sim}{v}(o, \underset{\sim}{r}') = 0$, we find in the transmitter plane

$$v_t(r) = \int_0^F d\xi \frac{\xi}{F} \frac{1}{n_0} \nabla n \left(\xi, r' = \frac{\xi}{F} r \right) \cdot \qquad [17]$$

The principle of operation of an ideal adaptive correction system is as follows. A sensor measures in some form or other the random phase front angle $\underset{\sim}{v}_t(\underset{\sim}{r})$, a processor then reverses the sign of $\underset{\sim}{v}_t(\underset{\sim}{r})$ and feeds the information to a phasor array that continuously changes the phase front of the outgoing laser beam to make $\underset{\sim}{v}(o,\underset{\sim}{r}) = -\underset{\sim}{v}_t(\underset{\sim}{r})$. If the latter condition is realized, the reversibility of the ray paths predicts that the phase front of the outgoing beam will gradually become undistorted and spherical as $z \rightarrow F$. Hence, the irradiance profile of the corrected beam should approach the diffraction limit.

In practice, the phase sensor and corrector have a discrete number of active elements. Therefore, the system cannot reproduce the function $-\underset{\sim}{v}_t(\underset{\sim}{r})$ on every point of the aperture of the outgoing beams and some form of spatial averaging must be taken into account. The true relation between the returned function $\underset{\sim}{v}_o(z)$ and the theoretical eq. 17 is particular to each system but it is believed that the following linear expression is sufficiently general to accommodate a wide class of applications:

$$v_o(r_i) = \frac{1}{\sigma_i} \iint_{\sigma_i} d^2\rho \; W_i(\rho) \left\{ v_b(r_i + \rho) - \Gamma_i(\rho)\, v_t(r_i + \rho) \right\}, \qquad [18]$$

where $\underset{\sim}{r}_i$ is the position vector of the i^{th} element, $\underset{\sim}{v}_b(\underset{\sim}{r}_i)$ is a random function representing the noise of the system, $\Gamma_i(\underset{\sim}{\rho})$ is the correlation coefficient between the true and the returned wave front angle for the i^{th} active element, $W_i(\underset{\sim}{\rho})$ is the window or weighting function associated with the i^{th} element, and σ_i is its surface.

The solution of the linearized eq. 15 for the outgoing phase front with boundary condition $\underset{\sim}{v}(o, \underset{\sim}{r}) = \underset{\sim}{v}_o(\underset{\sim}{r})$ is

$$\mathbf{v}(z, \mathbf{r}) = \frac{F}{F-z}\,\mathbf{v}_0\left(\frac{F}{F-z}\,\mathbf{r}\right) + \int_0^z d\zeta\,\frac{F-\zeta}{F-z}\,\nabla n\left(\zeta, \frac{F-\zeta}{F-z}\,\mathbf{r}\right). \qquad [19]$$

Using eqs. 17 to 19 and noting that $\xi = F - \zeta$, we have

$$\begin{aligned}
\mathbf{v}(z, \mathbf{r}_i) = {} & \frac{F}{F-z}\,\frac{1}{\sigma_i}\iint_{\sigma_i} d^2\rho\; W_i(\rho)\,\mathbf{v}_b\left(\frac{F}{F-z}\,\mathbf{r}_i + \rho\right) \\
& - \frac{1}{n_0\sigma_i}\iint_{\sigma_i} d^2\rho\; W_i(\rho)\,\Gamma_i(\rho)\int_0^F d\zeta\,\frac{F-\zeta}{F-z}\,\nabla n\left(\zeta, \frac{F-\zeta}{F-z}\,\mathbf{r}_i + \frac{F-\zeta}{F}\,\rho\right) \\
& + \frac{1}{n_0}\int_0^z d\zeta\,\frac{F-\zeta}{F-z}\,\nabla n\left(\zeta, \frac{F-\zeta}{F-z}\,\mathbf{r}_i\right) .
\end{aligned} \qquad [20]$$

An expression for the covariance of $\underset{\sim}{v}$ is easily derived from eq. 20. The method is well documented in Ref. 3. The simplifying hypotheses are that the correlation length of the turbulent refractive index is much smaller than the propagation distances of interest and that the noise $\underset{\sim}{v}_b$ is uncorrelated with the index n. Both these approximations are well justified in practice. The resulting solution for Kolmogorov's turbulence is then

$$\begin{aligned}
\langle \mathbf{v}(z, \mathbf{r}_i)\,\mathbf{v}(u, \mathbf{s}_j) \rangle = {} & \frac{F^2}{(F-z)(F-u)}\,\frac{1}{\sigma_i\sigma_j}\iint_{\sigma_i} d^2\rho \iint_{\sigma_j} d^2\tau\; W_i(\rho)\,W_j(\tau) \left\langle \mathbf{v}_b\left(\frac{F}{F-z}\,\mathbf{r}_i + \rho\right)\,\mathbf{v}_b\left(\frac{F}{F-u}\,\mathbf{s} + \tau\right) \right\rangle \\
& + \frac{1}{\sigma_i\sigma_j}\iint_{\sigma_i} d^2\rho \iint_{\sigma_j} d^2\tau\; W_i(\rho)\,W_j(\tau)\,\Gamma_i(\rho)\,\Gamma_j(\tau)\int_0^F \frac{d\zeta\,(F-\zeta)^2}{(F-z)(F-u)}\,\mathbf{M}\left[\frac{F-\zeta}{F-z}\,\mathbf{r}_i - \frac{F-\zeta}{F-u}\,\mathbf{s}_j + \frac{F-\zeta}{F}\,(\rho - \tau)\right] \\
& - \frac{1}{\sigma_i}\iint_{\sigma_i} d^2\rho\; W_i(\rho)\,\Gamma_i(\rho)\int_0^z \frac{d\zeta\,(F-\zeta)^2}{(F-z)(F-u)}\,\mathbf{M}\left[\frac{F-\zeta}{F-z}\,\mathbf{r}_i - \frac{F-\zeta}{F-u}\,\mathbf{s}_i + \frac{F-\zeta}{F}\,\rho\right] \\
& - \frac{1}{\sigma_i}\iint_{\sigma_i} d^2\tau\; W_i(\tau)\,\Gamma_i(\tau)\int_0^u \frac{d\zeta\,(F-\zeta)^2}{(F-z)(F-u)}\,\mathbf{M}\left[\frac{F-\zeta}{F-z}\,\mathbf{r}_i - \frac{F-\zeta}{F-u}\,\mathbf{s}_i - \frac{F-\zeta}{F}\,\tau\right] \\
& + \int_0^u \frac{d\zeta\,(F-\zeta)^2}{(F-z)(F-u)}\,\mathbf{M}\left[\frac{F-\zeta}{F-z}\,\mathbf{r}_i - \frac{F-\zeta}{F-u}\,\mathbf{s}_i\right].
\end{aligned} \qquad [21]$$

where

$$\underset{\approx}{M}(p) = \frac{2.43\, C_n^2}{n_0^2}\,\frac{1}{[p^2 + (.35\ell_0)^2]^{1/6}}\left\{\underset{\approx}{\delta} - \frac{1}{3}\,\frac{p^2}{p^2 + (.35\ell_0)^2}\,\underset{\sim}{a}_p\underset{\sim}{a}_p\right\} \cdot \qquad [22]$$

C_n is the index-structure constant, ℓ_o is the inner scale of turbulence, $\underset{\approx}{\delta}$ is the unit dyad (or, in tensor notation, the two-dimensional Kronecker delta) and $\underset{\sim}{a}_p$ is the unit vector along $\underset{\sim}{p}$.

The covariance of $\underset{\sim}{v}$, as defined by eq. 21, is a discrete function of the position vectors $\underset{\sim}{r}_i$ and $\underset{\sim}{s}_j$ of the active elements labeled i and j. This is very inconvenient to handle. Thus, to extend further the analytical treatment, we render eq. 21 continuous by assuming that the domain of the spatial integration over σ_i (or σ_j) remains symmetrical about any point $\underset{\sim}{r}$ (or $\underset{\sim}{s}$). In other words, we assume that the averaging effect of the active elements is invariant with position on the aperture. Finally, to simplify the results, the integration is performed over a circular region of effective radius r_e given by

$$r_e = (S/m\pi)^{1/2}, \qquad [23]$$

where S is the total area of the aperture and m, the number of active elements. This approximation appears reasonable for systems with continuous phase correctors such as deformable mirrors, but it should also give acceptable results even for segmented mirrors especially when the number of active elements is large.

As shown in Ref. 3, eq. 22 for $\underset{\approx}{M}(\underset{\sim}{p})$ is an empirical expression connecting two theoretical asymptotic formulas valid respectively for $p \ll \ell_o$ and $p \gg \ell_o$. It is therefore only consistent to proceed in the same fashion to determine the spatial averages of $\underset{\approx}{M}(\underset{\sim}{p})$: first, compute the averages in the two asymptotic limits and then, connect the results

by a single empirical continuous expression. For the present application, the weight and correlation functions $W_i(\rho)$ and $\Gamma_i(\rho)$ are taken to be unity. Defining

$$\Delta = \frac{F-\zeta}{F-z}\mathbf{r} - \frac{F-\zeta}{F-u}\mathbf{s}, \qquad [24]$$

we have for $\Delta >> \frac{F-\zeta}{F} r_e$

$$\overline{\mathbf{M}}_1^{(+)} = \frac{1}{\sigma^2}\iint_\sigma d^2\rho \iint_\sigma d^2\tau\, \mathbf{M}\left[\Delta + \frac{F-\zeta}{F}(\rho - \tau)\right] \simeq \frac{2.43\, C_n^2}{n_0^2}\,\frac{1}{\Delta^{1/3}}\left[\delta - \frac{1}{3}\mathbf{a}_\Delta \mathbf{a}_\Delta\right]. \qquad [25]$$

$$\overline{\mathbf{M}}_2^{(+)} = \frac{1}{\sigma}\iint_\sigma d^2\rho\, \mathbf{M}\left[\Delta + \frac{F-\zeta}{F}\rho\right] \simeq \frac{2.43\, C_n^2}{n_0^2}\,\frac{1}{\Delta^{1/3}}\left[\delta - \frac{1}{3}\mathbf{a}_\Delta \mathbf{a}_\Delta\right]. \qquad [26]$$

$$\overline{\mathbf{M}}_3^{(+)} = \frac{1}{\sigma}\iint_\sigma d^2\tau\, \mathbf{M}\left[\Delta - \frac{F-\zeta}{F}\tau\right] \simeq \frac{2.43\, C_n^2}{n_0^2}\,\frac{1}{\Delta^{1/3}}\left[\delta - \frac{1}{3}\mathbf{a}_\Delta \mathbf{a}_\Delta\right]. \qquad [27]$$

and for $\Delta << \frac{F-\zeta}{F} r_e$,

$$\overline{\mathbf{M}}_1^{(-)} \simeq \frac{2.43\, C_n^2}{n_0^2}\,\frac{\delta}{\sigma^2}\iint_\sigma d^2\rho \iint_\sigma d^2\tau \left\{\frac{(F-\zeta)^2}{F^2}|\rho - \tau|^2 + (.35\ell_0)^2\right\}^{-1/6}. \qquad [28]$$

Performing the integrations in eq. 28 and using $\sigma = \pi r_e^2$,

$$\overline{\mathbf{M}}_1^{(-)} \simeq \frac{2.43\, C_n^2}{n_0^2}\,\delta\left\{(.35\ell_0)^2 + 0.199\frac{(F-\zeta)^2}{F^2} r_e^2\right\}^{-1/6}. \qquad [29]$$

Similarly, we have

$$\overline{\mathbf{M}}_2^{(-)} = \overline{\mathbf{M}}_3^{(-)} \simeq \frac{2.43\, C_n^2}{n_0^2}\,\delta\left\{(.35\ell_0)^2 + 0.335\frac{(F-\zeta)^2}{F^2} r_e^2\right\}^{-1/6}. \qquad [30]$$

Then, the two asymptotic regions are connected by a single algebraic formula as follows:

$$\overline{M}(\Delta, L_i) = \frac{2.43\, C_n^2}{n_0^2} \frac{1}{[\Delta^2 + L_i^2]^{5/6}} \left\{ \delta - \frac{1}{3} \frac{\Delta^2}{\Delta^2 + L_i^2} a_\Delta a_\Delta \right\} . \qquad [31]$$

where i = 1, 2, 3 and

$$L_1^2 = \quad (.35\ell_0)^2 + 0.199 \frac{(F-\zeta)^2}{F^2} r_e^2 , \qquad [32a]$$

$$L_2^2 = L_3^2 = (.35\ell_0)^2 + 0.335 \frac{(F-\zeta)^2}{F^2} r_e^2 \cdot \qquad [32b,c]$$

Finally, from eqs. 21 and 31, the covariance of $\underset{\sim}{v}$ is given by

$$< v(z,r)\, v(u,s) > = \frac{F^2}{(F-z)(F-u)} \frac{1}{\sigma^2} \iint_\sigma d^2\rho \iint_\sigma d^2\tau < v_b\left(\frac{F}{F-z} r + \rho\right) \; v_b\left(\frac{F}{F-u} s + \tau\right) >$$
$$+ \int_0^F d\zeta \frac{(F-\zeta)^2}{(F-z)(F-u)} \overline{M}(\Delta, L_1) - \int_0^z d\zeta \frac{(F-\zeta)^2}{(F-z)(F-u)} \overline{M}(\Delta, L_2)$$
$$- \int_0^u d\zeta \frac{(F-\zeta)^2}{(F-z)(F-u)} \overline{M}(\Delta, L_3) + \int_0^u d\zeta \frac{(F-\zeta)^2}{(F-z)(F-u)} \overline{M}(\Delta, L_4) \cdot \qquad [33]$$

where, for symmetry of notation, we have defined

$$L_4^2 = (.35\ell_0)^2 \qquad [32d]$$

The contribution due to noise depends on the covariance of $\underset{\sim}{v}_b$ which is characteristic of the particular system under study. For the present general application, it is convenient to assume a homogeneous and isotropic noise, Gaussianly correlated with a e-folding radius equal to r_e, i.e.

$$\frac{1}{\sigma^2} \iint_\sigma d^2\rho \iint_\sigma d^2\tau < v_b\left(\frac{F}{F-z} r + \rho\right) \; v_b\left(\frac{F}{F-u} s + \tau\right) > = \frac{\sigma_b^2}{2} \delta \exp\left\{ - \left| \frac{F}{F-z} r - \frac{F}{F-u} s \right|^2 r_e^{-2} \right\} . \qquad [34]$$

The parameter σ_b^2 is the noise strength, i.e. the spatially averaged variance of the random angular error of the active elements. Equation 34 simplifies the algebra and should give results representative of a real system.

The expressions for the coefficients $\underset{\approx}{R}(z)$ and K(z) can now be obtained by substituting eqs. 33 and 34 in eqs. 10 and 11. The integration over $\underset{\sim}{s}$ is performed as described in Ref. 3. For the noise contributions, the complete integrals are done analytically. The results are expressed as follows:

$$\mathbf{R}(z) = \mathbf{R}_b(z) + \mathbf{R}_1(z) - \mathbf{R}_2(z) - \mathbf{R}_3(z) + \mathbf{R}_4(z), \qquad [35]$$

$$K(z) = K_b(z) + K_1(z) - K_2(z) - K_3(z) + K_4(z), \qquad [36]$$

where $\underset{\approx}{R}_b(z)$ and $K_b(z)$ are algebraic expressions of elementary transcendental functions to be given later in nondimensional variables and where

$$\mathbf{R}_i(z) = \frac{2.43\, C_n^2}{n_0^2}\,\delta \int_0^z du \int_0^{Y_i} d\zeta \frac{(F-\zeta)^2\, H(\gamma_i)}{L_i^{5/3}(F-z)(F+z-2u)}, \qquad [37]$$

$$K_i(z) = \frac{3.24\, C_n^2}{n_0^2} \int_0^z du \int_0^{Y_i} d\zeta \frac{(F-\zeta)^2\, G(\gamma_i)}{L_i^{7/3}(F-z)(F+z-2u)}, \qquad [38]$$

with

$$Y_1 = F\,;\; Y_2 = z\,;\; Y_3 = Y_4 = u, \qquad [39]$$

$$\gamma_i = \frac{-jk\, L_i^2}{2(z-u)} \; \frac{(F-u)(F+z-2u)}{(F-\zeta)^2}, \qquad [40]$$

$$G(\gamma) = \gamma^2 \left\{ \frac{1}{2} + 3\gamma + \left[\, 5/12 - \gamma - 3\gamma^2 \,\right] \frac{e^\gamma}{\gamma^{5/6}}\, \Gamma(5/6, \gamma) \right\}. \qquad [41]$$

$$H(\gamma) = \gamma \left\{ 1 + \left[\, 5/6 - \gamma \,\right] \frac{e^\gamma}{\gamma^{5/6}}\, \Gamma(5/6, \gamma) \right\}. \qquad [42]$$

$\Gamma(5/6,\gamma)$ is the incomplete Gamma function defined by eq. 6.5.20 of Ref. 6.

The coefficients $\underset{\approx}{R}(z)$ and K(z) of eqs. 35 and 36 constitute the principal result of this report. They permit the closure of the amplitude-moment equations and they model the effects of turbulence and of adaptive optics.

3.2 Jitter Model

Another phenomenon that contributes to beam divergence is jitter. Jitter arises from random vibrations of the transmitter platform which cause a random tilt of the outgoing phase front. We consider here the residual jitter which is left uncorrected by the adaptive system.

To determine the contributions of jitter to $\underset{\approx}{R}(z)$ and K(z), we proceed in a manner different to that used in the preceding section. The reason is that the phase and amplitude fluctuations resulting from jitter are correlated over the complete field of propagation which invalidates a basic hypothesis leading to eqs. 10 and 11. We therefore return to the defining constitutive relations given in Ref. 3, i.e.

$$< \mathbf{a}\nabla\cdot\mathbf{v} > = -\,\mathbf{K}(z) < \mathbf{A} >, \qquad [43]$$

$$< \mathbf{av} > \; = -\,\mathbf{R}(z) : \nabla < \mathbf{A} >, \qquad [44]$$

$$< \mathbf{aav} > \; = -\frac{1}{2}\mathbf{R}(z) : \nabla < \mathbf{aa} >, \qquad [45]$$

$$< \mathbf{aa^*v} > \; = -\frac{1}{2}\,\mathbf{Real}\,\{\,\mathbf{R}(z)\,\} : \nabla < \mathbf{aa^*} >, \qquad [46]$$

from which we will derive $\underset{\approx}{R}(z)$ and K(z) by substituting the specialized jitter solutions for $\underset{\sim}{v}$ and a.

Let α be the tilt angle due to jitter measured from the axis of propagation. In the notation of this report, we thus have in the transmitter plane

$$\mathbf{v}_\alpha(0, \mathbf{r}) = \alpha\, \mathbf{e}_\alpha , \qquad [47]$$

where the subscript α refers to the jitter contribution and $\underset{\sim}{e}_\alpha$ is a unit vector of random direction in the plane normal to the propagation axis. Then, from eq. 19, the solution $\underset{\sim}{v}_\alpha(z, \underset{\sim}{r})$ is

$$\mathbf{v}_\alpha(z, \mathbf{r}) = \frac{F}{F - z}\, \alpha\, \mathbf{e}_\alpha \cdot \qquad [48]$$

Equation 48 shows that $\underset{\sim}{v}_\alpha(z, \underset{\sim}{r})$ is uniform in the transverse plane, i.e. independent of the position r.

From Ref. 3, the implicit solution for the fluctuating amplitude caused by jitter is

$$a_\alpha(z, \mathbf{r}) = \frac{-jk}{2\pi}\int_0^z \frac{du}{(u - z)}\iint_{-\infty}^{\infty} d^2\mathbf{s}\, \mathbf{v}_\alpha(u, \mathbf{s}) \cdot \nabla_s A(u, \mathbf{s}) \exp\left\{ \frac{jk}{2(z - u)}\, \frac{F - z}{F - u}\left|\frac{F - z}{F - u}\mathbf{r} - \mathbf{s}\right|^2 \right\} \cdot \qquad [49]$$

Since $\underset{\sim}{\nabla} \cdot \underset{\sim}{v}_\alpha = 0$, the amplitude fluctuations are caused by the random angular motion of the beam as a whole. In other words, jitter produces amplitude modulations on the same scale as that of the average beam. Hence, we can assume that the scale of $\underset{\sim}{\nabla}_s$ A, at least the part correlated with $\underset{\sim}{v}_\alpha$, is greater than $\sqrt{(z-u)\lambda}$, so that $\underset{\sim}{\nabla}_s A(u,\underset{\sim}{s})$ can be taken out of the integral over s and evaluated along the line $\underset{\sim}{s} = \dfrac{F-u}{F-z}\, \underset{\sim}{r}$, i.e.

$$\nabla_s A(u, \mathbf{s}) = \frac{F - z}{F - u}\, \nabla_r A\left(u, \frac{F - u}{F - z}\mathbf{r}\right) \cdot \qquad [50]$$

This, in fact, is the geometrical optics approximation. In the framework of this approximation,

$$A\left(u, \frac{F-u}{F-z}\mathbf{r}\right) = \frac{F-z}{F-u} A(z, \mathbf{r}), \qquad [51]$$

and eq. 50 becomes

$$\nabla_s A(u, s) = \frac{(F-z)^2}{(F-u)^2} \nabla_r A(z, \mathbf{r}) \cdot \qquad [52]$$

Finally, using eqs. 48 and 52 in eq. 49 and performing the integration, we find

$$\mathbf{a}_\alpha(z, \mathbf{r}) = -\alpha\, z\, \mathbf{e}_\alpha \cdot \nabla A(z, \mathbf{r}) \cdot \qquad [53]$$

Equations 48 and 53 are the jitter solutions for $\underset{\sim}{v}$ and a which can now be used to derive an expression for $\langle \underset{\sim}{v} a \rangle_\alpha$. Multiplying eq. 48 by 53 and taking the ensemble average, we find

$$\langle va \rangle_\alpha = \frac{-Fz}{(F-z)} \langle \alpha^2 \mathbf{e}_\alpha \mathbf{e}_\alpha \cdot \nabla A \rangle \cdot \qquad [54]$$

Assuming that $\underset{\sim}{e}_\alpha$ is statistically independent of α and A as is the case in most applications and neglecting third-order moments between α and A which are $O(\langle \alpha^3 \rangle)$, we can simplify eq. 54 as follows:

$$\langle va \rangle_\alpha = \frac{-Fz}{(F-z)} \langle \alpha^2 \rangle \langle \mathbf{e}_\alpha \mathbf{e}_\alpha \rangle \cdot \nabla \langle A \rangle \cdot \qquad [55]$$

Finally, if $\underset{\sim}{e}_\alpha$ is uniformly distributed, $\langle \underset{\sim}{e}_\alpha \underset{\sim}{e}_\alpha \rangle = \underset{\approx}{\delta}/2$ and eq. 55 becomes

$$\langle va \rangle_\alpha = \frac{-Fz}{(F-z)} \frac{\langle \alpha^2 \rangle}{2} \delta \cdot \nabla \langle A \rangle \cdot \qquad [56]$$

To derive the expression for $\langle \underset{\sim}{v}aa\rangle_\alpha$, we multiply eq. 53 by $a\underset{\sim}{v}_\alpha(z,r)$ and take the ensemble average. Using eq. 48 for $\underset{\sim}{v}_\alpha$ and assuming that α and A are near Gaussian random functions, we find to the same order of precision as for eq. 56

$$< \mathbf{vaa} >_\alpha = \frac{-\mathbf{Fz}}{(\mathbf{F}-\mathbf{z})} \frac{<\alpha^2>}{4} \boldsymbol{\delta} \cdot \nabla < \mathbf{aa} > \cdot \qquad [57]$$

Similarly,

$$< \mathbf{vaa^*} >_\alpha = \frac{-\mathbf{Fz}}{(\mathbf{F}-\mathbf{z})} \frac{<\alpha^2>}{4} \boldsymbol{\delta} \cdot \nabla < \mathbf{aa^*} >, \qquad [58]$$

and, since $\underset{\sim}{\nabla}\cdot\underset{\sim}{v}_\alpha = 0$,

$$< \mathbf{a}\nabla \cdot \mathbf{v} >_\alpha = 0 . \qquad [59]$$

Therefore, from comparison between eqs. 43 to 46 and 50 to 59, it follows that

$$\mathbf{R}_\alpha(z) \approx \frac{\mathbf{Fz}}{(\mathbf{F}-\mathbf{z})} \frac{\sigma_\alpha^2}{2} \boldsymbol{\delta} . \qquad [60]$$

$$\mathbf{K}_\alpha(z) \approx 0 \cdot \qquad [61]$$

The coefficients $\underset{\approx}{R}_\alpha(z)$ and $K_\alpha(z)$ model the effect of beam jitter. The parameter $\sigma_\alpha^2 = \langle\alpha^2\rangle$ is the variance of the uncorrected tilt angle of the outgoing phase front caused by transmitter vibrations.

3.3 Partial Coherence Model

Real laser sources, especially high-power lasers, do not generally have complete coherence. They are partially coherent which causes a beam divergence greater than the diffraction-limited divergence. As

shown in Ref. 7, the property of partial coherence is modeled by a statistically homogeneous random phase ψ_c over the source plane. With the notation of eq. 1, this is mathematically represented as follows:

$$A(0,\mathbf{r}) = \sqrt{I(\mathbf{r})}\exp\{j\,\Psi c(\mathbf{r})\}\,, \qquad [62]$$

where $I(\underset{\sim}{r})$ is the irradiance profile of the source. The degree of coherence is measured by the correlation function of $A(o,\underset{\sim}{r})$, i.e.

$$\frac{< A(0,\mathbf{r})\,A^*(0,\mathbf{s}) >}{[I(\mathbf{r})\,I(\mathbf{s})]^{1/2}} = < \exp\{j\,(\Psi c(\mathbf{r}) - \Psi c(\mathbf{s}))\} > \cdot \qquad [63]$$

If we choose that Ψ_c has a Gaussian probability density function with zero mean, as is done in Ref. 7, eq. 63 becomes

$$\frac{< A(0,\mathbf{r})\,A^*(0,\mathbf{s}) >}{[I(\mathbf{r})\,I(\mathbf{s})]^{1/2}} = \exp\left\{ -\frac{1}{2} < (\Psi c(\mathbf{r}) - \Psi c(\mathbf{s}))^2 > \right\} \cdot \qquad [64]$$

It is also customary, e.g. Refs. 7-10, to consider a Gaussian correlation function for $A(o,\underset{\sim}{r})$, i.e.

$$\frac{< A(0,\mathbf{r})\,A^*(0,\mathbf{s}) >}{[I(\mathbf{r})\,I(\mathbf{s})]^{1/2}} = \exp\left\{ -\frac{|\mathbf{r}-\mathbf{s}|^2}{2r_c^2} \right\}, \qquad [65]$$

where r_c is called the coherence radius of the source. Although the hypotheses of Gaussian statistics for Ψ_c and of a Gaussian correlation function for A are not essential, they permit a simplified analytic treatment of the phenomenon. Hence, from eqs. 64 and 65 it follows that

$$< (\Psi c(\mathbf{r}) - \Psi c(\mathbf{s}))^2 > = \frac{|\mathbf{r}-\mathbf{s}|^2}{r_c^2}\,. \qquad [66]$$

The random phase Ψ_c of eq. 62 can be considered a boundary condition to the geometrical phase $k\phi$ of eq. 1. Since the equations of the present model deal with the gradient of the phase, we define, in accordance with our previous notation, the random vector

$$\mathbf{v}_c(0, \mathbf{r}) = \frac{1}{k} \nabla \Psi c(\mathbf{r}) \cdot \qquad [67]$$

Then, from eq. 66, we obtain

$$< \mathbf{v}_c(0, \mathbf{r})\, \mathbf{v}_c(0, \mathbf{s}) > = \frac{1}{k^2 r_c^2} \delta \cdot \qquad [68]$$

We note from eq. 68 that the covariance of $\chi_c(o,\mathbf{r})$ is uniform in the transverse plane, i.e. independent of $\mathbf{r}$. This situation is mathematically identical to jitter. Therefore, by replacing $<\alpha^2>$ by $2/k^2 r_c^2$ as indicated by eqs. 47 and 68, the results of the preceding section are applicable without further modifications. Thus, with reference to eqs. 60 and 61, the effect of partial coherence is modeled by the coefficients

$$\mathbf{R}_c(z) = \frac{Fz}{(F - z)} \; \frac{1}{k^2 r_c^2} \delta, \qquad [69]$$

$$\mathbf{K}_c(z) = 0. \qquad [70]$$

The degree of coherence of a source is often defined as the ratio q of its far-field divergence to that of a fully coherent source with the same irradiance profile. It can easily be shown, for a Gaussian source with an irradiance e-folding radius equal to r_o, that

$$r_c^2 = \frac{2 r_0^2}{q^2 - 1} \cdot \qquad [71]$$

This simple relation provides a practical means of estimating the coherence radius r_c of a real source.

4.0 METHOD OF SOLUTION

We have derived in the preceding sections the relations required to close the system of partial differential equations for the solution of the average irradiance and the irradiance variance of optical or infrared beams propagating in turbulence. The model includes the effect of adaptive optics, that of jitter and that of partial coherence of the source. We will now assemble these results and propose a method of solution.

In the treatment of complex problems such as the one considered in this report, it is important to nondimensionalize the governing equations. This generally permits a substantial reduction of the number of parameters on which the solutions depend; actually, the number of parameters is thus reduced to its essential minimum. There results a saving in computational effort: the same solution being applicable to different physical situations. The solutions of the nondimensionalized system are called similarity solutions and the nondimensional parameters, the similarity parameters.

The propagation distance z is normalized by the length scale

$$z_A = n_0^{12/11} C_n^{-12/11} k^{-7/11}; \qquad [72]$$

the transverse coordinate, by the radius r_o of the source irradiance profile; the average amplitude, by the square root of the on-axis source irradiance; and the second-order amplitude moments, by the

on-axis source irradiance. Performing the normalization of the dependent and independent variables in eqs. 7 to 9, we obtain the following set of nondimensional partial differential equations:

$$\left(\frac{\partial}{\partial\eta} + \frac{\rho}{\eta - f}\frac{\partial}{\partial\rho}\right) < A > - \frac{jb}{2}\nabla_\rho^2 < A > - bR(\eta)\nabla_\rho^2 < A > = -\frac{< A >}{(\eta - f)} - \frac{1}{2}K(\eta) < A >, \qquad [73]$$

$$\left(\frac{\partial}{\partial\eta} + \frac{\rho}{\eta - f}\frac{\partial}{\partial\rho}\right) < aa^* > - \frac{b^2 f}{(f - \eta)}\frac{\eta}{2}\nabla_\rho^2 < aa^* > - \frac{b}{2}\mathrm{Real}\left[R(\eta)\right]\nabla_\rho^2 < aa^* >$$

$$= -\frac{2 < aa^* >}{(\eta - f)} + \mathrm{Real}\left[K(\eta)\right] < A > < A >^* + 2b\,\mathrm{Real}\left[R(\eta)\right]\nabla_\rho < A > \cdot \nabla_\rho < A >^*, \qquad [74]$$

$$\left(\frac{\partial}{\partial\eta} + \frac{\rho}{\eta - f}\frac{\partial}{\partial\rho}\right) < aa > - \frac{jb}{4}\nabla_\rho^2 < aa > - \frac{b}{2}R(\eta)\nabla_\rho^2 < aa > + jT(\eta) < aa >$$

$$= -\frac{2 < aa >}{(\eta - f)} + K(\eta) < A > < A > + 2b\,R(\eta)\nabla_\rho < A > \cdot \nabla_\rho < A >. \qquad [75]$$

The coefficients $T(\eta)$, $R(\eta)$ and $K(\eta)$ are given by

$$T(\eta) = (0.15 - 0.01\,j)\frac{f - \eta/2}{f - \eta}\left\{\begin{matrix} 1/\eta\,;\,\eta \leq 1 \\ \eta\,;\,\eta > 1 \end{matrix}\right\}, \qquad [76]$$

$$R(\eta) = R_c(\eta) + R_\alpha(\eta) + R_b(\eta) + R_1(\eta) - R_2(\eta) - R_3(\eta) + R_4(\eta), \qquad [77]$$

$$K(\eta) = K_b(\eta) + K_1(\eta) - K_2(\eta) - K_3(\eta) + K_4(\eta), \qquad [78]$$

where

$$R_c(\eta\,;\,f, P) = \frac{P}{2}\,\frac{f\eta}{f - \eta}, \qquad [79]$$

$$R_\alpha(\eta\,;\,f, J) = \frac{J}{2}\,\frac{f\eta}{f - \eta}, \qquad [80]$$

$$R_b(\eta\,;\,f, \eta_1, B) = \frac{j\,B\eta_1}{4}\,\frac{f}{(f - \eta)}\left\{\left[\frac{f - \eta}{f} - \frac{Y}{2fZ}\right]\frac{V}{Q} + \frac{U}{2fZ}\right\}. \qquad [81]$$

$$K_b(\eta\,;\,f, \eta_1, B) = \frac{j\,B}{2}\,\frac{f}{(f - \eta)}\left\{\frac{(2XZ - Y^2)\eta - XY}{fZQ\,(X + Y\eta + Z\eta^2)}\right.$$

$$+ \frac{(Y\eta + 2X)}{Q(X + Y\eta + Z\eta^2)}\,\frac{f - \eta}{f} + \frac{Y}{fZQ} - \frac{2(f - \eta)}{Qf} + \frac{U}{2fZ}$$

$$\left. + \left[\frac{Y}{Q}\,\frac{(f - \eta)}{f} - \frac{2X}{fQ} - \frac{Y}{2fZ} + \frac{f - \eta}{f}\right]\frac{V}{\sqrt{Q}}\right\}. \qquad [82]$$

with

$$X = \frac{j\,\eta_1}{2}\;\frac{(f-\eta)^2}{f^2},$$

$$Y = \frac{3}{2}\;\frac{j\eta_1}{f}\;\frac{(f-\eta)}{f} - 1,$$

$$Z = j\eta_1/f,$$

$$Q = Y^2 - 4XZ,$$

$$U = \ln\left[(X + Y\eta + Z\eta^2)/X\right],$$

$$V = \ln\left[\frac{2Z\eta + Y - \sqrt{Q}}{2Z\eta + Y + \sqrt{Q}} \cdot \frac{Y + \sqrt{Q}}{Y - \sqrt{Q}}\right],$$

and

$$K_i(\eta; f, \eta_0, \eta_1) = 3.24 \int_0^\eta dy \int_0^{y_i} dx \, \frac{(f-x)^2\, G(\gamma_i)}{\ell_i^{7/6}\,(f-\eta)\,(f+\eta-2y)}, \qquad [83]$$

$$R_i(\eta; f, \eta_0, \eta_1) = 2.43 \int_0^\eta dy \int_0^{y_i} dx \, \frac{(f-x)^2\, H(\gamma_i)}{\ell_i^{1/6}\,(f-\eta)\,(f+\eta-2y)}, \qquad [84]$$

with

$$\ell_1 = \eta_0 + 0.199\,\frac{(f-x)^2}{f^2}\,\eta_1;$$

$$\ell_2 = \ell_3 = \eta_0 + 0.335\,\frac{(f-x)^2}{f^2}\,\eta_1;\; \ell_4 = \eta_0,$$

$$y_1 = f;\; y_2 = \eta;\; y_3 = y_4 = y,$$

$$\gamma_i = -j\,\frac{\ell_i}{2(\eta-y)}\;\frac{(f-y)\,(f+\eta-2y)}{(f-x)^2}.$$

The nondimensional independent variables are

$$\eta = z/z_A;\; \rho = r/r_0\,. \qquad [85a,b]$$

The beam is characterized by the similarity parameters

$$f = F/z_A;\; b = z_A/kr_0^2\,. \qquad [86a,b]$$

the turbulent medium, by the parameter

$$\eta_0 = 0.123\, k\ell_0^2/z_A, \quad [87]$$

the adaptive optics, by the parameter

$$\eta_1 = kr_c^2/z_A \quad [88]$$

the noise of the active elements, by the parameter

$$B = kz_A \sigma_\xi^2, \quad [89]$$

the jitter of the transmitting optics, by the parameter

$$J = kz_A \sigma_\alpha^2, \quad [90]$$

and the partial coherence of the source, by the parameter

$$P = 2z_A/kr_c^2\,. \quad [91]$$

The differential eqs. 73 to 75 together with the constitutive eqs. 76 to 84 for the closure coefficients constitute the propagation model of this report. These equations are sufficient to solve for the average irradiance, eq. 13, and the irradiance variance, eq. 14, of laser beams propagating in turbulence and corrected by adaptive optics; they also include modeling of the effects of jitter and partial coherence. Solutions can be computed after the initial profile and the various similarity parameters defined by eqs. 86 to 91 have been specified.

General solutions of eqs. 73 to 75 can be worked out in terms of Green's functions but this leads to complicated multiple integrals that are troublesome and lengthy to evaluate for specific applications. We find it much more convenient to solve the finite-difference version of eqs. 73 to 75. This approach is straightforward and involves no particular difficulties except perhaps in the near vicinity of $\eta = f$.

For originally Gaussian beams, we find that the irradiance profile is very nearly self-similar. This interesting property suggests an algorithm that minimizes the computational difficulties related to the change of the transverse scale with the propagation distance. Indeed, for beams focused at $\eta = f$, the diameter decreases with η until it reaches a minimum value at some $\eta < f$. If correction is effective, the minimum diameter can be very small relative to the characteristic radius r_o. Hence, solving eqs. 73 to 75 on a homogeneous grid requires that the latter be chosen fine enough to resolve the sharpest profile and the method becomes inefficient for the greatest part of the propagation domain. This is further complicated by the fact that the value of the minimum diameter is not known a priori except for the extremum diffractional limit which is generally too small. However, the property of near self-similarity provides a convenient way around this problem as outlined by the following method.

The dependent variables are written as follows:

$$< A > = F_1(\eta)\, P_1(\eta, \xi = \mathbf{p}/\sigma(\eta))\,, \qquad [92]$$

$$< aa^* > = F_2(\eta)\, P_2(\eta, \xi)\,, \qquad [93]$$

$$< aa > = F_3(\eta)\, P_3(\eta, \xi)\,. \qquad [94]$$

If the solutions were truly self-similar, the functions P_i would be independent of η and depend only on ξ. However, for near self-similar solutions, the functional representation given by eqs. 92 to 94 becomes advantageous since the scale variations are almost completely accounted for by the functions $F_i(\eta)$ and $\sigma(\eta)$ of one independent variable only. It is important to note, however, that the eqs. 92 to 94 do not alter or restrict the generality of the problem, they are simply used to ease the numerical calculations despite the apparently more complex algebra.

Substituting the eqs. 92 to 94 for <A>, <aa*> and <aa> in the eqs. 73 to 75 and assuming circular symmetry, we obtain the following equations for the functions $P_i(\eta,\xi)$:

$$\frac{\partial P_1}{\partial \eta} - b\,\frac{[\mathrm{Real}\,\{R(\eta)\} + bf\eta/(f-\eta)]}{\sigma^2(\eta)}\left[\xi\,\frac{\partial P_1}{\partial \xi} + 2\,P_1\right]$$

$$- b\,\frac{[R(\eta) + j/2]}{\sigma^2(\eta)}\nabla_\xi^2 P_1 = 0\,, \tag{95}$$

$$\frac{\partial P_2}{\partial \eta} - b\,\frac{[\mathrm{Real}\,\{R(\eta)\} + bf\eta/(f-\eta)]}{\sigma^2(\eta)}\left[\xi\,\frac{\partial P_2}{\partial \xi} + 2\,P_2 + \frac{1}{2}\nabla_\xi^2 P_2\right]$$

$$= \frac{\mathrm{Real}\,\{K(\eta)\}}{F_2(\eta)}\left|F_1(\eta)\,P_1\right|^2 + 2b\,\frac{\mathrm{Real}\,\{R(\eta)\}}{\sigma^2(\eta)\,F_2(\eta)}\left|F_1(\eta)\,\frac{\partial P_1}{\partial \xi}\right|^2. \tag{96}$$

$$\frac{\partial P_3}{\partial \eta} - b\,\frac{[\mathrm{Real}\,\{R(\eta)\} + bf\eta/(f-\eta)]}{\sigma^2(\eta)}\left[\xi\,\frac{\partial P_3}{\partial \xi} + 2\,P_3\right] - b\,\frac{[R(\eta) + j/2]}{2\sigma^2(\eta)}\nabla_\xi^2 P_3$$

$$= \frac{K(\eta)\,F_1^2(\eta)}{F_3(\eta)}\,P_1^2 + 2b\,\frac{R(\eta)\,F_1^2(\eta)}{\sigma^2(\eta)\,F_3(\eta)}\left(\frac{\partial P_1}{\partial \xi}\right)^2. \tag{97}$$

where

$$\sigma^2(\eta) = \frac{(f-\eta)^2}{f^2} + b^2\eta^2 + 2b(f-\eta)^2\int_0^\eta \frac{\mathrm{Real}\,\{R(\zeta)\}}{(f-\zeta)^2}\,d\zeta\,, \tag{98}$$

$$F_1(\eta) = \frac{(f-\eta)}{f\sigma^2(\eta)}\exp\left\{-\frac{1}{2}\int_0^\eta K(\zeta)\,d\zeta\right\}\,, \tag{99}$$

$$F_2(\eta) = 1/\sigma^2(\eta)\,, \tag{100}$$

$$F_3(\eta) = \frac{1}{\sigma^2(\eta)}\exp\left\{-j\int_0^\eta \Pi(\zeta)\,d\zeta\right\}\,. \tag{101}$$

A rapid inspection of the eqs. 95 to 97 for the functions P_i reveals that the terms involving differentiation with respect to ξ are all multiplied by the similarity parameter b. For most applications, b is small and, therefore, the resulting functions P_i experience little changes in their transverse scale. This is particularly true for Gaussian

beams which satisfy the equation $(\xi \frac{\partial P_1}{\partial \xi} + 2P_1 + 1/2\, \nabla_\xi^2 P_1 = 0)$ at $\eta=0$. Consequently, the partial differential equations 95 to 97 can be efficiently and easily solved by finite-difference techniques on a homogeneous grid. The most important scale changes occur in the eqs. 98 to 101 for $\sigma^2(\eta)$ and $F_i(\eta)$ which necessitate only three straightforward numerical integrations. Finally, since the functions P_i are very nearly self-similar, the beam divergence can be calculated with good accuracy from eq. 98 alone. Inspection of the latter together with eq. 77 for $R(\eta)$ shows that the often used method of approximating beam divergence by summing the squares of the contributions due to geometrical optics, diffraction, turbulence, jitter and partial coherence is verified by our model.

5.0 RESULTS

Our propagation model was tested against experimental data in Refs. 2 and 3. Excellent agreement was demonstrated with both simulation and atmospheric measurements on widely different scales. These comparisons were carried out for propagation in turbulence without correction, jitter or conditions of partial coherence. In this report, we present calculation results that simulate the effects of adaptive optics but no data are yet available for direct verification. Nevertheless, the solutions are consistent and informative and they show interesting properties that should promote future experimention.

For the present calculations, we consider two beams, one at 10.6 μm and the other at 3.8 μm, propagating under the same experimental conditions. The atmospheric turbulence is assumed homogeneous with a very strong index structure constant $C_n = 10^{-6} m^{-1/3}$ and an inner scale $\ell_o = 0.01$ m. The influence of the inner scale on the solutions is small and the exact value of ℓ_o is not important. The sources are Gaussian with an e-folding irradiance diameter $2r_o = 0.5$ m and the out-

going beams are focused at F = 3 km. The adaptive mirror is circular with a diameter equal to 1 m and contains a variable number of active elements. The effective area of the active elements is simply taken as the total area of the mirror divided by the number of elements. Finally, to reduce the multiplicity of solutions, partial coherence and beam jitter are neglected. This has little consequence for the purpose of this report since their principal effect consists in lowering the attainable power-density limit with trivial changes to the structure of the solutions.

Figures 2 and 3 provide examples of the types of solutions calculated with the present model. They show the normalized beam radius defined as follows:

$$w(\eta) = \int_0^\infty \rho^3 < I(\eta,\rho) > d\rho \Big/ \int_0^\infty \rho < I(\eta,\rho) > d\rho \qquad [102]$$

plotted against the propagation distance. Two curves are drawn: one without correction and the other with correction. Figure 2 pertains to the 10.6-μm wavelength and Fig. 3, to 3.8 μm. These calculations show that the focusing power at F = 3 km, which was almost completely lost because of turbulence spreading, is significantly restored by a 36-element adaptive mirror.

To collect a greater number of calculation results, the Strehl number is plotted versus the propagation distance in Figs. 4 and 5 for 10.6 μm and 3.8 μm respectively. The Strehl number is defined as the ratio of the average on-axis irradiance calculated in turbulence to the diffraction-limited irradiance. A value of unity means that the correction is complete and that the diffraction limit is attained. When no correction is applied, Figs. 4 and 5 reveal that the Strehl number continuously decreases with the propagation distance up to the focal plane where it reaches values as low as 0.0082 and 0.00085 respectively. With correction, the ratio decreases a little more rapidly at the

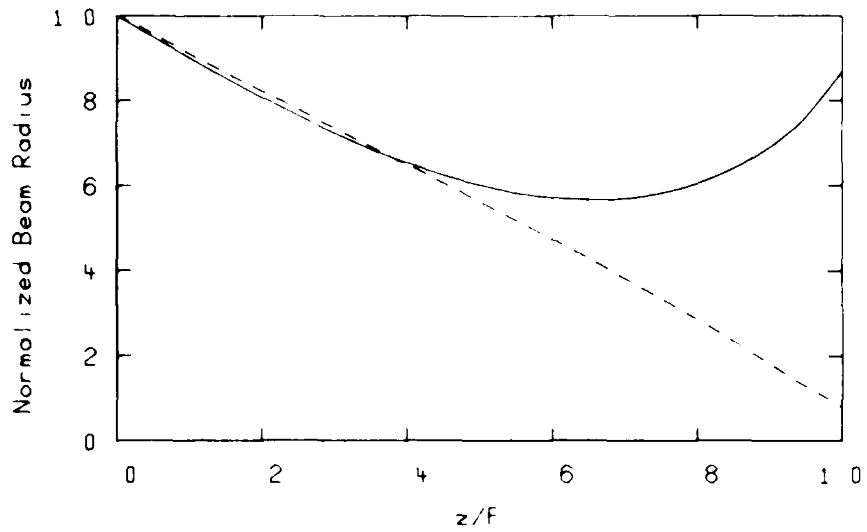

FIGURE 2 - Computed normalized beam radius versus propagation distance for a 10.6-μm Gaussian beam. The other parameters are: $C_n = 10^{-6}m^{-1/3}$; ℓ_o = 10 mm; r_o = 0.25 m; F = 3 km; diameter of the deformable mirror D = 1 m; and system noise σ_b = 0. Continuous line: no correction; dashed line: correction with m = 36 active elements.

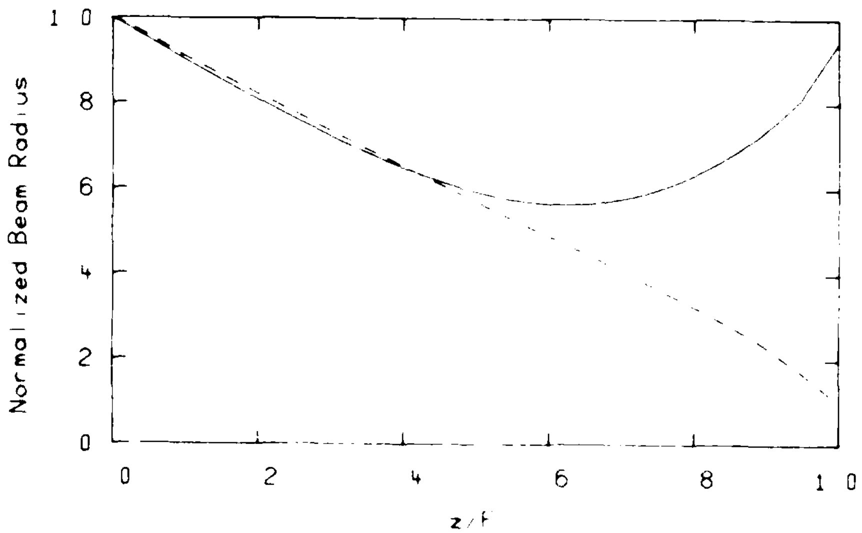

FIGURE 3 - Computed normalized beam radius versus propagation distance for a 3.8-μm Gaussian beam. Continuous line: no correction; dashed line: correction with m = 36 active elements. C_n, ℓ_o, r_o, F, D and σ_o as in Fig. 2.

beginning but much more slowly as z = F is approached. If the number of active elements is sufficiently large, the ratio passes through a minimum at an intermediate propagation distance to rise again toward the focal plane. Ultimately, the diffraction limit is attained at z = F and little improvement at shorter distances is gained by increasing the number of active elements. It takes more elements to achieve the same diffraction-limit condition at 3.8 μm than at 10.6 μm.

To demonstrate the correction efficiency of adaptive systems, Figs. 6 and 7 show the power-density gain in the focal plane as a function of the number of active elements. The gain is defined as the ratio of the on-axis focal plane average irradiance with correction to the irradiance calculated without correction. The gain increases monotonically with the number of active elements and becomes quite substantial with relatively few elements. It is interesting to note that the gain below the diffraction limit is of the same order at both wavelengths. The diffraction limit of about 20 dB at 10.6 μm is achieved with 60 elements whereas 200 elements are not sufficient to reach the same condition at 3.8 μm.

Real systems suffer from noise which degrades their performance. To illustrate this effect, two additional gain curves are plotted in each of Figs. 6 and 7 for noise levels σ_b = 10 μrad and 31.6 μrad respectively. The parameter σ_b is the standard deviation of the random error in the wave front shape returned by the active elements. It is shown that a noise below 10 μrad causes little degradation but that substantial gain reduction occurs at σ_b = 31.6 μrad. These results assume the particular and simple noise model defined by eq. 34. Although they should not be quantitatively applied to real systems without further verification, they are indicative of the magnitude of the effect of the random errors of the active elements.

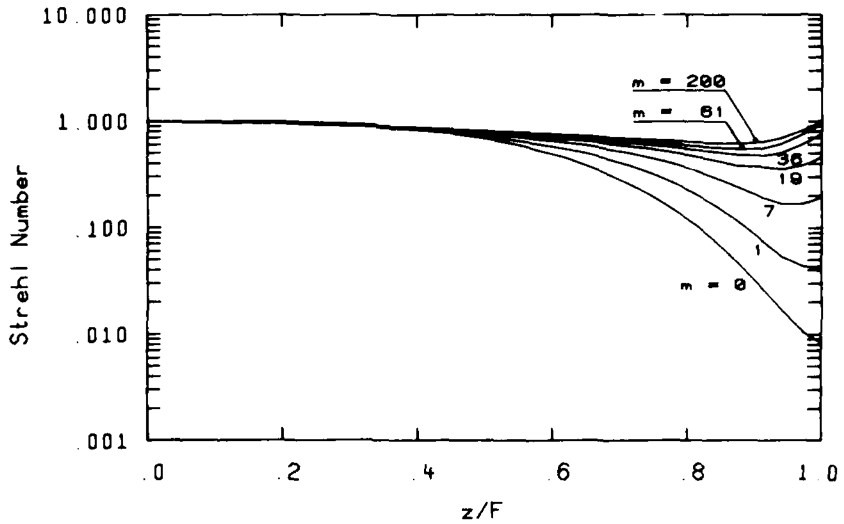

FIGURE 4 - Computed Strehl number versus propagation distance for a 10.6-μm Gaussian beam. C_n, ℓ_o, r_o, F, D and σ_b as in Fig. 2.

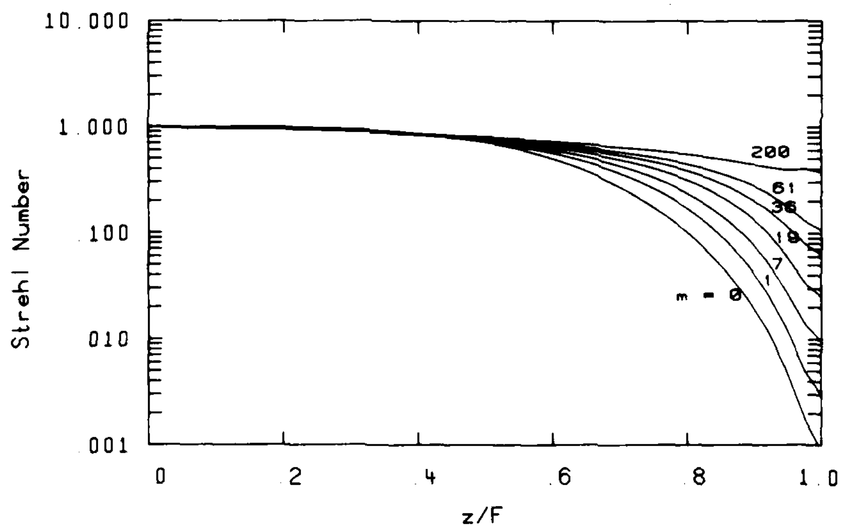

FIGURE 5 - Computed Strehl number versus propagation distance for a 3.8-μm Gaussian beam. C_n, ℓ_o, r_o, F, D and σ_b as in Fig. 2.

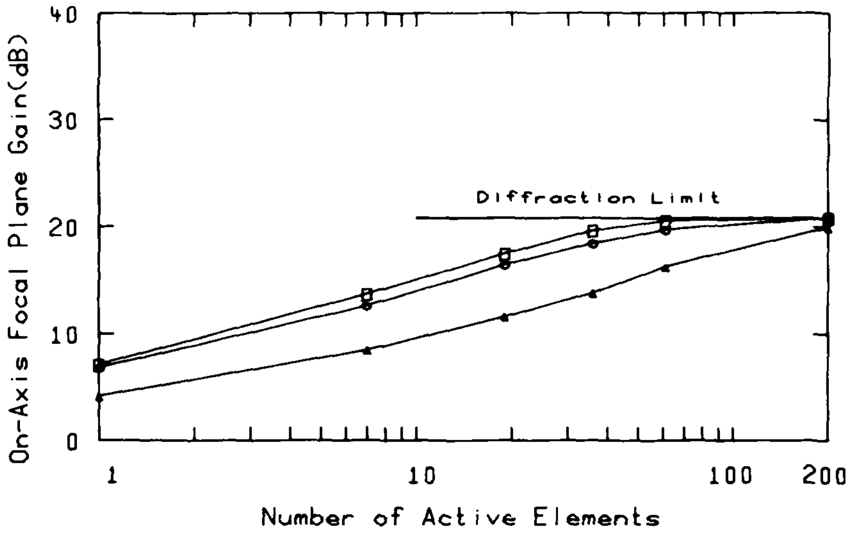

FIGURE 6 - Computed gain in on-axis focal-plane power density versus the number of active elements for a 10.6-μm Gaussian beam, □: $\sigma_b = 0$; 0: $\sigma_b = 10$ μrad; and Δ: $\sigma_b = 31.6$ μrad. The horizontal line defines the diffractional limit. C_n, ℓ_o, r_o, F and D as in Fig. 2.

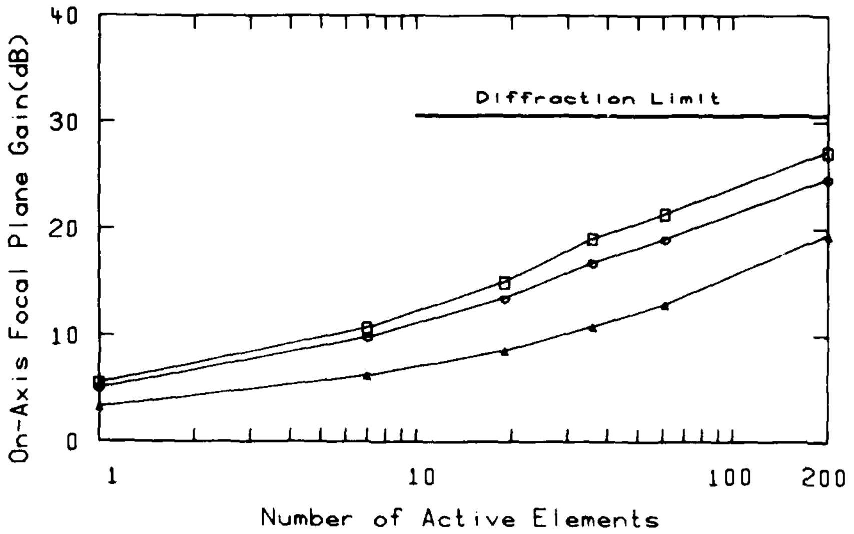

FIGURE 7 - Computed gain in on-axis focal-plane power density versus the number of active elements for a 3.8 μm Gaussian beam, □: $\sigma_b = 0$; 0: $\sigma_b = 10$ μrad; and Δ: $\sigma_b = 31.6$ μrad. The horizontal line defines the diffractional limit. C_n, ℓ_o, r_o, F and D as in Fig. 2.

The effectiveness of the adaptive system at the two wavelengths, λ = 10.6 μm and 3.8 μm, is compared in Figs. 8, 9 and 10 for the noise levels σ_b = 0, 10 and 31.6 μrad respectively. In these figures, the on-axis focal-plane average irradiance normalized by the on-axis transmitter irradiance is plotted versus the number of active elements. The conditions of operation are the same at both wavelengths so that the comparison is performed in terms of absolute quantities. In general, the turbulence-induced beam spread is greater at shorter wavelengths. As shown in Figs. 8-10, this remains valid in the presence of adaptive optics up to a certain limit. Indeed, the 10.6-μm beam consistently gives the highest focal-plane power density until the 10.6-μm diffraction limit is attained. Beyond that point, increasing the number of active elements no longer affects the 10.6-μm beam but continues to improve the performance of the shorter 3.8-μm wavelength beam. The cross-over point where 3.8 μm becomes more advantageous than 10.6 μm is approximately 60 elements at σ_b = 0, 90 elements at σ_b = 10 μrad, and greater than 200 elements at σ_b = 31.6 μrad. Of course, these numbers apply to the special case studied in this report. For weaker turbulence, the model predicts that the cross-over point occurs at a smaller number of active elements.

The on-axis focal plane scintillation strength is plotted in Figs. 11-13 versus the number of active elements for σ_b = 0, 10 and 31.6 μrad respectively. The scintillation strength is defined as the ratio $\sigma_I/\langle I \rangle$ where σ_I is the irradiance standard deviation at one point and $\langle I \rangle$, the average irradiance at the same point. Two curves are drawn in each figure corresponding to the two wavelengths λ = 10.6 and 3.8 μm. These results show that the scintillation remains strong even when the average-irradiance beam profile is near diffraction limited; a reduction relative to the no-correction level of at best 25% is observed for the case of Figs. 11-13. Such residual irradiance fluctuations are experimentally observed, for example, in Fig. 6 of Ref. 11.

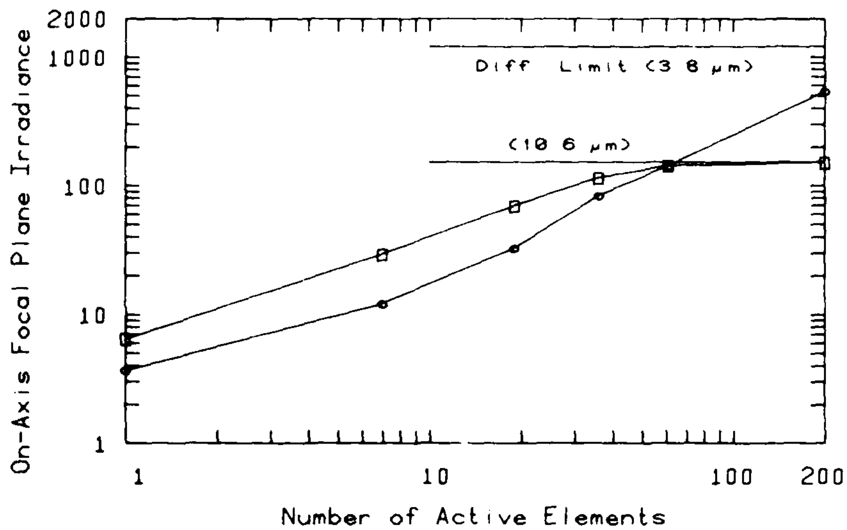

FIGURE 8 - Comparison of the computed on-axis focal-plane average irradiance versus the number of active elements for the two wavelengths λ = 10.6 μm (□) and λ = 3.8 μm (0) without system noise, i.e. $\sigma_b = 0$. The horizontal lines define the respective diffractional limits. C_n, ℓ_o, r_o, F and D as in Fig. 2.

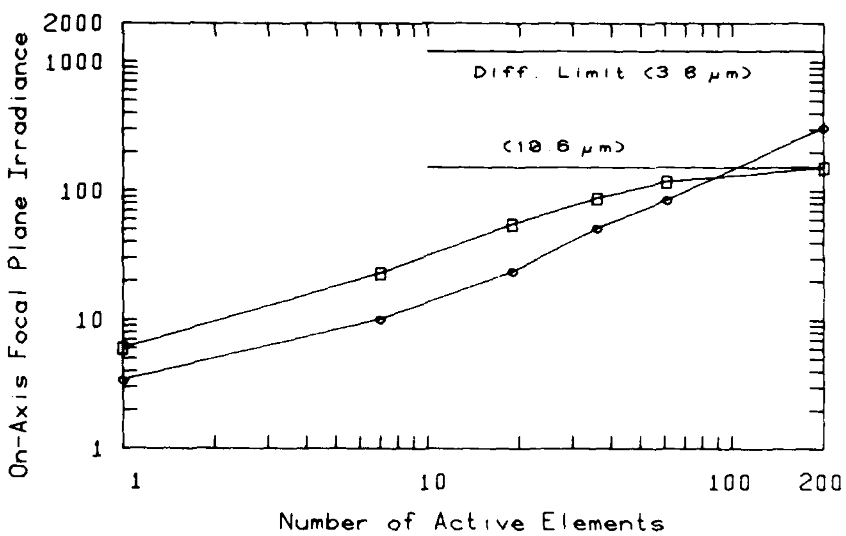

FIGURE 9 - Comparison of the computed on-axis focal-plane average irradiance versus the number of active elements for the two wavelengths λ = 10.6 μm (□) and λ = 3.8 (0) with system noise σ_b = 10 μrad. The horizontal lines define the respective diffractional limits. C_n, ℓ_o, r_o, F and D as in Fig. 2.

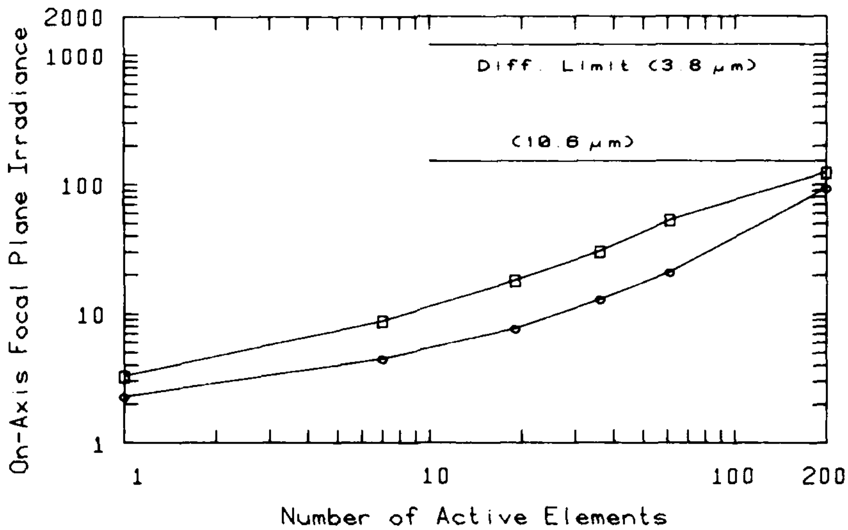

FIGURE 10 - Comparison of the computed on-axis focal-plane average irradiance versus the number of active elements for the two wavelengths λ = 10.6 μm (□) and λ = 3.8 μm (0) with system noise σ_b = 31.6 μrad. The horizontal lines defines the respective diffractional limits. C_n, ℓ_o, r_o, F and D as in Fig. 2.

Theoretically, a nonzero scintillation level is not incompatible with a diffraction-limited beam profile; irradiance fluctuations can indeed propagate on a smooth phase front. Moreover, it can be shown from the model equations that correction for both beam spreading and scintillation would require the adaptive system not only to reproduce the conjugate of the phase of the spherical wave retro-reflected by the target glint, but to return its full 'spatial' complex conjugate including the amplitude modulations. This is possible with the nonlinear optical technique of phase conjugation (e.g. four-wave mixing) which has been demonstrated in recent years (Ref. 12). However, many developments are still required for the method to be technically applicable to high-power laser beams.

Finally, the 10.6-μm curves of Figs. 8-9 and 11-12 show that the scintillation is minimum at the number of elements just needed to achieve diffraction-limited beam spread. Therefore, the latter condition is the optimum operating condition for the type of adaptive systems studied here. Increasing the number of active elements not only produces no further gain in power density, but it worsens the level of residual scintillation.

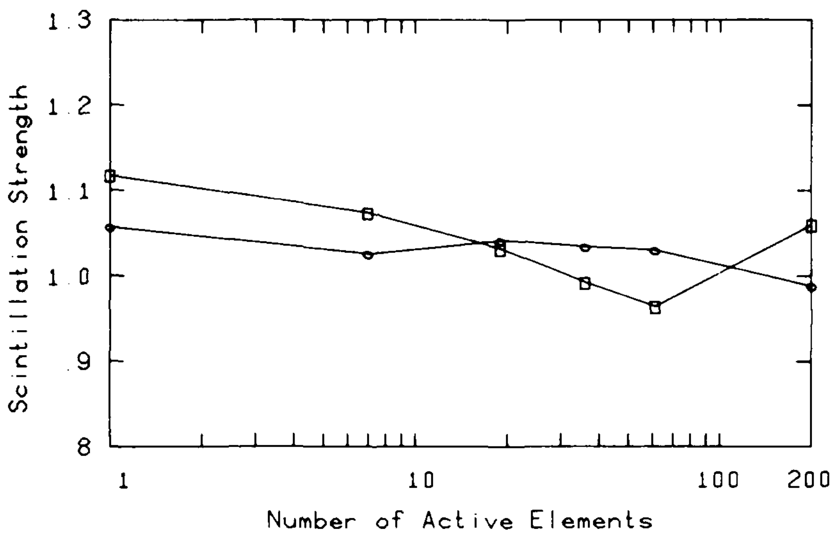

FIGURE 11 - Comparison of the computed on-axis focal-plane scintillation strength, $\sigma_I/\langle I \rangle$, versus the number of active elements for the two wavelengths λ = 10.6 μm (□) and λ = 3.8 μm (0) without system noise, i.e. $\sigma_b = 0$. C_n, ℓ_o, r_o, F and D as in Fig. 2.

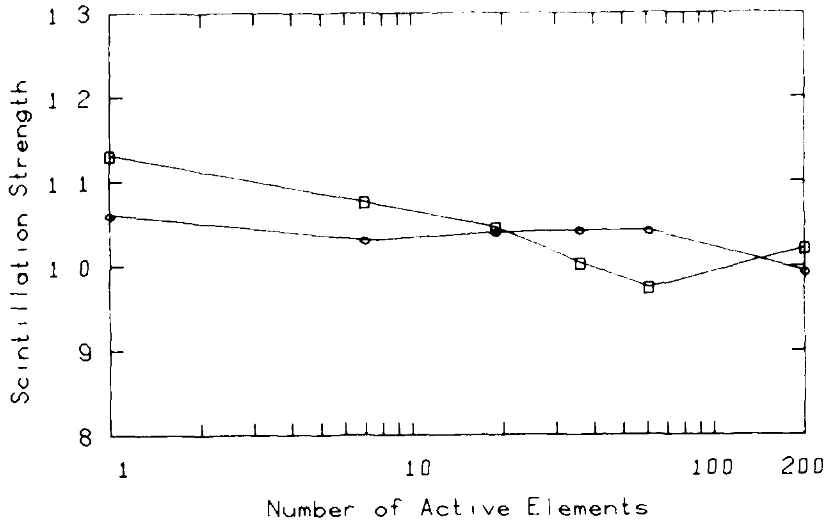

FIGURE 12 - Comparison of the computed on-axis focal-plane scintillation strength, $\sigma_I/<I>$, versus the number of active elements for the two wavelengths λ = 10.6 μm (□) and λ = 3.8 μm (0) with system noise σ_b = 10 μrad. C_n, ℓ_o, r_o, F and D as in Fig. 2.

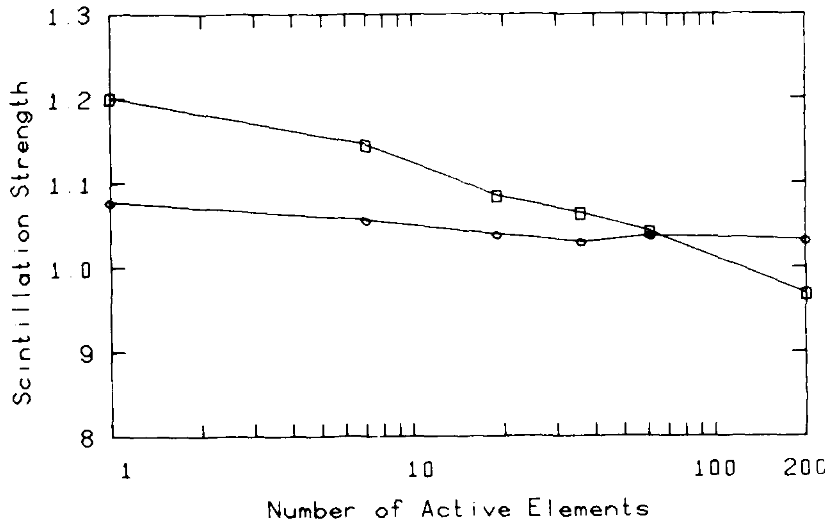

FIGURE 13 - Comparison of the computed on-axis focal-plane scintillation strength, $\sigma_I/<I>$, versus the number of active elements for the two wavelengths λ = 10.6 μm (□) and λ = 3.8 μm (0) with system noise σ_b = 31.6 μrad. C_n, ℓ_o, r_o, F and D as in Fig. 2.

6.0 CONCLUSION

The calculation results of the preceding section show that our turbulence propagation model can efficiently predict the average irradiance and the irradiance variance profiles of adaptively corrected laser beams traveling in atmospheric turbulence. The solutions are computed by a straightforward finite-difference technique and are uniformly valid at arbitrary scintillation levels.

The cases studied demonstrate the potential of adaptive optics to correct for turbulence beam spreading. Gain in focal-plane power density of the order of 20 dB relative to uncorrected propagation appears possible with a practical number of active elements even in strong turbulence and in the presence of system noise. Gains of this magnitude are certainly advantageous whatever the application. The model should thus be very useful for the design of practical systems and for scaling test results to expected operational conditions.

One aspect of adaptive optics not fully accounted for in the proposed model is phase retrieval. Here, we have assumed, as shown by eq. 18, that the phase front angle returned by the adaptive system is the spatial average, over the active element surface area, of a quantity which is linearly related to the true angle of the conjugate phase front of the spherical wave reflected by the target glint. In real applications, the relation can be more complex than eq. 18 and can also be affected by scintillation and target speckles. Thus, eq. 18 will likely need more investigation if it is applied to specific adaptive systems. However, for the time being, it remains a satisfactory approximation to work out estimates of the corrective effects of adaptive optics.

7.0 ACKNOWLEDGMENTS

The author is indebted to Dr M. Gravel for many valuable discussions and suggestions.

8.0 REFERENCES

1. Bissonnette, L.R., " Average Irradiance and Irradiance Variance of Laser Beams in Turbulent Media", DREV R-4104/78, May 1978, UNCLASSIFIED.

2. Bissonnette, L.R., "Modelling of Laser Beam Propagation in Atmospheric Turbulence", pp. 73-94, Proceedings of the Second International Symposium on Gas-Flow and Chemical Lasers, John F. Wendt, Editor, Hemisphere Publishing Corporation, Washington, D.C., 1979.

3. Bissonnette, L.R., "Focused Laser Beams in Turbulent Media", DREV R-4178/80, December 1980, UNCLASSIFIED

4. Hardy, John W., "Active Optics: A New Technology for the Control of Light", Proc. IEEE, Vol. 66, No. 6, pp. 651-697, June 1978.

5. Bissonnette, L.R. and Wizinowich, P.L., "Probability Distribution of Turbulent Irradiance in a Saturation Regime", Applied Optics, Vol. 18, No. 10, pp. 1590 - 1599, 15 May 1979.

6. Abramowitz, M. and Stegun, I.A., "Handbook of Mathematical Functions", Dover Publications, New York, 1965.

7. Wang, S.C.H. and Plonus, M.A., "Optical Beam Propagation for a Partially Coherent Source in the Turbulent Atmosphere", J. Opt. Soc. Am., Vol. 69, No. 9, pp. 1297-1304, Sept. 79.

8. Foley, J.T. and Zubairy, M.S., "The Directionality of Gaussian Schell-Model Beams", Optics Commun., Vol. 26, No. 3, pp. 297-300, Sept. 78.

9. Wolf, E. and Collett, E., "Partially Coherent Sources which Produces the Same Far-Field Intensity Distribution as a Laser", Optics Commun., Vol. 25, No. 3, pp. 293 - 296, June 78.

10. Wolf, E. and Carter W.H., "Angular Distribution of Radiant Intensity from Sources of Different Degrees of Spatial Coherence", Optics Commun., Vol. 13, No. 3, pp . 205-209, March 1975.

11. Pearson, James E., "Atmospheric Turbulence Compensation Using Coherent Optical Adaptive Techniques", Appl. Opt., Vol. 15, No. 3, pp. 622-631, March 1976.

12. Yariv, A., "Phase Conjugate Optics and Real-Time Holography", IEEE J. Quantum Electron., QE-14, No. 9, pp. 650-660, Sept. 1978. see also comments in QE-15, No. 6, pp. 523-525, June 1979.

CRDV R-4200/81 (NON CLASSIFIE)

Bureau - Recherche et Développement, MDN, Canada.
CRDV, C.P. 8800, Courcelette, Qué. GOA 1RO

"Modèle de propagation dans la turbulence de faisceaux laser corrigés par une optique adaptable" par L. Bissonnette

Ce rapport décrit un modèle mathématique pour la solution du problème de propagation de faisceaux laser se déplaçant dans l'atmosphère turbulente et corrigés par une optique adaptable. Celle-ci est simulée à l'aide d'une relation mathématique simple mais suffisamment générale pour représenter la plupart des systèmes existants. Le modèle tient compte également des effets de vibration du faisceau et de cohérence partielle de la source. La méthode permet de prédire les profils de l'intensité moyenne et de la variance de l'intensité pour des niveaux arbitraires de scintillation. On présente quelques solutions typiques pour des faisceaux de longueur d'onde de 3.8 et 10.6 μm. Ces résultats illustrent les performances, après propagation dans la turbulence, d'un système d'optique adaptable en fonction de la longueur d'onde, du nombre d'éléments actifs et du niveau de bruit. (NC)

CRDV R-4200/81 (NON CLASSIFIE)

Bureau - Recherche et Développement, MDN, Canada.
CRDV, C.P. 8800, Courcelette, Qué. GOA 1RO

"Modèle de propagation dans la turbulence de faisceaux laser corrigés par une optique adaptable" par L. Bissonnette

Ce rapport décrit un modèle mathématique pour la solution du problème de propagation de faisceaux laser se déplaçant dans l'atmosphère turbulente et corrigés par une optique adaptable. Celle-ci est simulée à l'aide d'une relation mathématique simple mais suffisamment générale pour représenter la plupart des systèmes existants. Le modèle tient compte également des effets de vibration du faisceau et de cohérence partielle de la source. La méthode permet de prédire les profils de l'intensité moyenne et de la variance de l'intensité pour des niveaux arbitraires de scintillation. On présente quelques solutions typiques pour des faisceaux de longueur d'onde de 3.8 et 10.6 μm. Ces résultats illustrent les performances, après propagation dans la turbulence, d'un système d'optique adaptable en fonction de la longueur d'onde, du nombre d'éléments actifs et du niveau de bruit. (NC)

CRDV R-4200/81 (NON CLASSIFIE)

Bureau - Recherche et Développement, MDN, Canada.
CRDV, C.P. 8800, Courcelette, Qué. GOA 1RO

"Modèle de propagation dans la turbulence de faisceaux laser corrigés par une optique adaptable" par L. Bissonnette

Ce rapport décrit un modèle mathématique pour la solution du problème de propagation de faisceaux laser se déplaçant dans l'atmosphère turbulente et corrigés par une optique adaptable. Celle-ci est simulée à l'aide d'une relation mathématique simple mais suffisamment générale pour représenter la plupart des systèmes existants. Le modèle tient compte également des effets de vibration du faisceau et de cohérence partielle de la source. La méthode permet de prédire les profils de l'intensité moyenne et de la variance de l'intensité pour des niveaux arbitraires de scintillation. On présente quelques solutions typiques pour des faisceaux de longueur d'onde de 3.8 et 10.6 μm. Ces résultats illustrent les performances, après propagation dans la turbulence, d'un système d'optique adaptable en fonction de la longueur d'onde, du nombre d'éléments actifs et du niveau de bruit. (NC)

CRDV R-4200/81 (NON CLASSIFIE)

Bureau - Recherche et Développement, MDN, Canada.
CRDV, C.P. 8800, Courcelette, Qué. GOA 1RO

"Modèle de propagation dans la turbulence de faisceaux laser corrigés par une optique adaptable" par L. Bissonnette

Ce rapport décrit un modèle mathématique pour la solution du problème de propagation de faisceaux laser se déplaçant dans l'atmosphère turbulente et corrigés par une optique adaptable. Celle-ci est simulée à l'aide d'une relation mathématique simple mais suffisamment générale pour représenter la plupart des systèmes existants. Le modèle tient compte également des effets de vibration du faisceau et de cohérence partielle de la source. La méthode permet de prédire les profils de l'intensité moyenne et de la variance de l'intensité pour des niveaux arbitraires de scintillation. On présente quelques solutions typiques pour des faisceaux de longueur d'onde de 3.8 et 10.6 μm. Ces résultats illustrent les performances, après propagation dans la turbulence, d'un système d'optique adaptable en fonction de la longueur d'onde, du nombre d'éléments actifs et du niveau de bruit. (NC)

DREV R-4200/81 (UNCLASSIFIED)

Research and Development Branch, DND, Canada.
DREV, P.O. Box 8800, Courcelette, Que, GOA 1RO

"Propagation Model of Adaptively Corrected Laser Beams in Turbulence"
by L. Bissonnette

This report describes a mathematical model for solving the propagation problem of laser beams traveling in atmospheric turbulence and corrected by adaptive optics. The modeling of the adaptive optics is mathematically simple but sufficiently general to encompass the majority of the existing systems. The model also includes the effects of beam jitter and partial coherence of the source. The method allows the prediction of the average irradiance and the irradiance variance beam profiles for arbitrary scintillation levels. Typical solutions are presented for 3.8- and 10.6-μm laser beams. These results illustrate the performance, after propagation in turbulence, of an adaptive system as a function of the wavelength, the number of active elements and the noise level. (U)

DREV R-4200/81 (UNCLASSIFIED)

Research and Development Branch, DND, Canada.
DREV, P.O. Box 8800, Courcelette, Que, GOA 1RO

"Propagation Model of Adaptively Corrected Laser Beams in Turbulence"
by L. Bissonnette

This report describes a mathematical model for solving the propagation problem of laser beams traveling in atmospheric turbulence and corrected by adaptive optics. The modeling of the adaptive optics is mathematically simple but sufficiently general to encompass the majority of the existing systems. The model also includes the effects of beam jitter and partial coherence of the source. The method allows the prediction of the average irradiance and the irradiance variance beam profiles for arbitrary scintillation levels. Typical solutions are presented for 3.8- and 10.6-μm laser beams. These results illustrate the performance, after propagation in turbulence, of an adaptive system as a function of the wavelength, the number of active elements and the noise level. (U)

DREV R-4200/81 (UNCLASSIFIED)

Research and Development Branch, DND, Canada.
DREV, P.O. Box 8800, Courcelette, Que, GOA 1RO

"Propagation Model of Adaptively Corrected Laser Beams in Turbulence"
by L. Bissonnette

This report describes a mathematical model for solving the propagation problem of laser beams traveling in atmospheric turbulence and corrected by adaptive optics. The modeling of the adaptive optics is mathematically simple but sufficiently general to encompass the majority of the existing systems. The model also includes the effects of beam jitter and partial coherence of the source. The method allows the prediction of the average irradiance and the irradiance variance beam profiles for arbitrary scintillation levels. Typical solutions are presented for 3.8- and 10.6-μm laser beams. These results illustrate the performance, after propagation in turbulence, of an adaptive system as a function of the wavelength, the number of active elements and the noise level. (U)

DREV R-4200/81 (UNCLASSIFIED)

Research and Development Branch, DND, Canada.
DREV, P.O. Box 8800, Courcelette, Que, GOA 1RO

"Propagation Model of Adaptively Corrected Laser Beams in Turbulence"
by L. Bissonnette

This report describes a mathematical model for solving the propagation problem of laser beams traveling in atmospheric turbulence and corrected by adaptive optics. The modeling of the adaptive optics is mathematically simple but sufficiently general to encompass the majority of the existing systems. The model also includes the effects of beam jitter and partial coherence of the source. The method allows the prediction of the average irradiance and the irradiance variance beam profiles for arbitrary scintillation levels. Typical solutions are presented for 3.8- and 10.6-μm laser beams. These results illustrate the performance, after propagation in turbulence, of an adaptive system as a function of the wavelength, the number of active elements and the noise level. (U)

END

DATE
FILMED

3-82

DTIC

FILMED

8